Precision Engineering 55 (2019) 144–153

Contents lists available at ScienceDirect

Precision Engineering

journal homepage: www.elsevier.com/locate/precision

Modelling and investigation of material removal profile for computer controlled ultra-precision polishing☆

Lijuan Ren, Guangpeng Zhang*, Lu Zhang, Zhen Zhang, Yumei Huang

School of Mechanical and Precision Instrumental Engineering, Xi'an University of Technology, Xi'an, 710048, China

ARTICLE INFO

Keywords:
Material removal profile
Deviation characteristics
Free-form surface polishing

ABSTRACT

Computer controlled ultra-precision polishing (CCUP) is widely used for high-precision surface finish processing with high form accuracy and good surface finish. CCUP is a deterministic material removal process based on the surface error-profile and the removal characteristic of the polishing tool. Material removal profile is often used to characterize the material removed in polishing process. Deviation phenomenon is a newly detected feature of the material removal profile which may contribute to the non-negligible form error of the polished surface. In this paper, the material removal model is established on the basis of Preston equation to obtain a better understanding of the characteristics of material removal in surface polishing. Firstly, contact stress model is established using Hertz contact theory. Then, relative velocity in the contact area is analyzed using geometric methods which can directly reflect the difference of the velocity of points in the contact area. Finally, single factor analysis and Taguchi method are used to investigate the influence of polishing parameters on the deviation feature of material removal profile and to provide a way for parameter optimization. The simulation and experiment results indicate that the proposed method can describe the deviation features well and parameter optimization strategies are provided in the conclusions.

1. Introduction

Free-form surfaces are widely used in many industries with high surface quality required [1,2], such as engine blades, aspheric optical lenses, and the surface of the inner cavity of an injection mould. As a final machining process, polishing is typically used to remove cusps and stripes left on free-from surfaces and improve the surface roughness. CCUP is widely used for high-precision surface finish processing [3] which is a deterministic material removal process based on the surface error-profile and the removal characteristic of the polishing tool and characterized by the removal characteristics of the polishing tool [4]. Much research has been performed regarding process modelling [5–7], process parameters optimization [8–11], etc., but far from complete.

The amount of material removed during the polishing process is affected not only by the polishing conditions, but also the physical and geometric characteristics of the polishing tool and the polished part [12]. Material removal profile (MRP) is generally used to characterize the material removal feature. MRP prescribes the amount of material removed from the surface along a direction orthogonal to the tool path as a polishing tool is moved through the surface [13]. Zhang et al. introduced a wear index for polishing to relate the material removal to the polishing conditions based on the Archard wear equation, and developed an approach for calculating the MRP of polishing using a soft tool with fixed abrasives. A convex/concave surface is polished using a cylindrical/spherical tool with the tool axis parallel to the common tangent plane of the tool and part surface and the MRP obtained from simulations and experiments are parabolic [14]. However, interference occurs regularly with the tool axis parallel to the common tangent plane in polishing process. Tam et al. focused on the effect of the path curvature on the MRP. Simulation results indicate that the MRP is skewed and the location of the maximum material removal depth shifts toward the centre of the curvature of the tool path as the radius of the curvature is decreased [15]. This is the first time that the deviation phenomenon of the MRP is put forward, but only the curvature radius of the tool path is taken into consideration. The deviation characteristics of the MRP for free abrasive polishing of flat specimen using a sub-aperture pad were analyzed by Cheng Fan et al. [16]. Polishing parameters, including not only the process parameters, but also the abrasive grain size, polishing slurry properties, topographical parameters of the sub-aperture pad, as well as the tool path curvature, were taken into this proposed model.

☆ This paper was recommended by Associate Editor Christopher Tyler.

* Corresponding author. School of Mechanical and Precision Instrumental Engineering, Xi'an University of Technology, No. 5, Jinhua Road, Xi'an, 710048, China.
E-mail addresses: xkk19881120@163.com (L. Ren), gpzhang@xaut.edu.cn (G. Zhang), 18700935326@163.com (L. Zhang), z1184621439@163.com (Z. Zhang), hymxaut@163.com (Y. Huang).

https://doi.org/10.1016/j.precisioneng.2018.08.020
Received 11 April 2018; Received in revised form 7 August 2018; Accepted 28 August 2018
Available online 05 September 2018
0141-6359/

The theoretical and experimental profiles showed a deviation towards the centre of the tool path curvature, which is attributed to the longer dwelling time in the contact area near the curvature centre. Cao ZC et al. studied the material removal characteristics of bonnet polishing theoretically and experimentally [17]. The results indicate that the MRP is asymmetrical in the X-cross-section, but no in-depth analysis related to the asymmetric material removal profile. An asymmetrical profile of material removed leads to non-uniform material removal on the surface. The uniformity of the material removed affects the finishing, and in some cases, the accuracy of the polished surface form. Non-uniform removal may appear as waviness or texture on the polished surface [18]. It may also contribute to the non-negligible form error of the polished surface [19]. However, how the polishing parameters affect the deviation characteristics of the asymmetrical distribution of the material removed has not been reported in publication.

This study focuses on the influence law of the polishing parameters on the deviation characteristics of material removal profile. Firstly, the contact stress modelling of the contact area was established using the Hertz contact theory. Then, the relative velocity distribution in the contact area was analyzed using a geometric method, and a normalized mathematical model of the relative velocity was implemented, taking the deformation of the polishing tool into consideration. Thirdly, the material removal model of fixed spot polishing was build on the basis of the Preston equation. Simulations and experiments were conducted, focusing on the effects of the polishing conditions on the deviation characteristics of the MRP. The purpose of this paper is to provide a quantitative description of the relationship between the major polishing parameters and the deviation characteristics of the MRP, and to provide theoretical basis for polishing parameter optimization and trajectory planning ensuring an uniform material removal on the polished surface.

2. Material removal profile modelling

The Preston equation is a currently used mathematical model to describe the law of material removal through polishing [19,20]. Preston stated that the material removal rate is determined based on the interactions among the pressure distribution, relative velocity, dwelling time and the Preston coefficient, which is related to the physical and geometric characteristics of the polishing tool and workpiece [21]. The Preston equation can be written as:

$$H(x, y) = \Delta t \cdot K \cdot P(x, y) \cdot V(x, y) \tag{1}$$

where $H(x, y)$ is the material removal depth at point (x, y) in the contact area, Δt is the dwelling time, K is the Preston coefficient, $P(x, y)$ is the instantaneous positive pressure at point (x, y) in the contact area, $V(x, y)$ is the relative velocity between the tool head and the workpiece surface at point (x, y), and x and y are coordinates relative to the x- and y-axes with the origin at the centre of the contact area.

In this study, the contact stress and relative velocity distribution in the polishing contact area are analyzed in this section based on following assumptions: 1) the polishing tool is an elastic and smooth spherical surface neglect micro-protrusion of the abrasive grains, 2) the part surface is absolutely rigid, 3) the surface of the part has two identical principle radii of curvature.

2.1. Contact stress modelling

It is the contact stress that determines the quality of the polished part not the force exerted on the polishing tool [22]. The contact situation between the polishing tool and the polished part is complex because of the complicated topography of the abrasives on the tool surface [23] and the changing geometry of the part surface. Previous research work [4,20] shows that the distribution of contact pressure appears to be in the shape of a Gaussian function, which is obtained using statistics. Hertz contact theory is extensively used to establish the pressure distribution model [15,22,24]. A contact model between two curved surfaces was described by Hertz in 1927. Based on the Hertz contact theory, the contact area between two curved surfaces with different principle radii of curvature is an ellipse. The contact model of two curved surface is shown in Fig. 1. Fig. 1 (a) is a schematic of two curved surfaces with different principle radii of curvature pressed against each other. Fig. 1(b) is a sketch of the elliptic contact area. R_1, R_1', R_2 and R_2' are two principle radii of curvature at the point of contact of the two curved surfaces respectively. P is the normal load exerted on the two bodies. a and b are the semi-minor axis and semi-major axis of the elliptic contact area respectively.

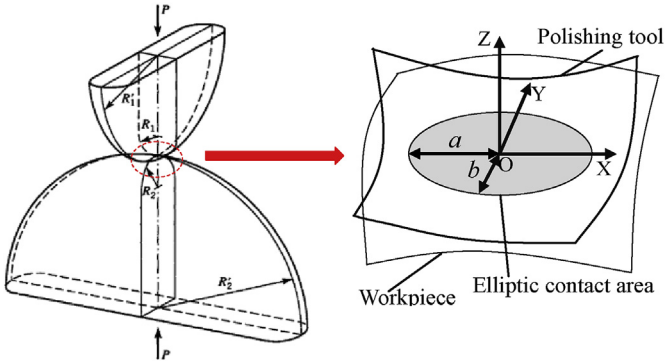

Fig. 1. Contact model of two curved surfaces (a) Two curved surfaces pressed against each other [25] and (b) Elliptic contact area.

According to the Hertz contact theory, the contact stress modelling in the contact area can be expressed as follows:

$$P(x, y) = R_e E^* \sqrt{\left(\frac{3F}{2\pi R_e E^*}\right)^{2/3} - x^3 - y^2} \tag{2}$$

The expressions of E^* and R_e are given as:

$$\frac{1}{R_e} = \frac{1}{A + B} \tag{3}$$

$$\frac{1}{E^*} = \frac{1 - \upsilon_1^2}{E_1} + \frac{1 - \upsilon_2^2}{E_2} \tag{4}$$

where E_1, E_2, υ_1, and υ_2 are the elastic modulus and Poisson's ratio of the tool head and the polished part respectively. In addition, A and B are positive constants that depend on the principal radii of curvature of the two curved surfaces at the point of contact.

2.2. Relative velocity modelling

Relative velocity is the velocity difference between the rotating tool and the workpiece. For spherical polishing tool, the relative velocity is the product of the rotation speed and the rotation radius, also known as linear velocity. Before contact with the part, the linear velocity of points on the spherical surface varies because of the different rotation radius shown as Fig. 2. After the tool is pressed on a stationary part, the relative velocity distribution becomes more complex caused by the deformation of the flexible tool.

The polishing tool is pressed and rotated on the workpiece with a spherical surface as shown in Fig. 2. The tool is always tilted by an angle to avoid the zero velocity of the centre point in the contact area. δ is the deformation of the polishing tool. ω is the rotation speed of the polishing tool around the tool axis. S is the spot size of polishing. Tilt angle is defined as angle between tool axis and the Z axis. O_T is the Geometric centre of the spherical tool. O_A and O_B are the rotation centre of points A and B at the contact area, respectively. Therefore, O_AA and O_BB are the rotation radius of point A and B, and the length of rotation radius of point in the contact area varies from O_AA to O_BB. For free-form surface, the distribution is much more complicated due to the variation of the radii of curvature.

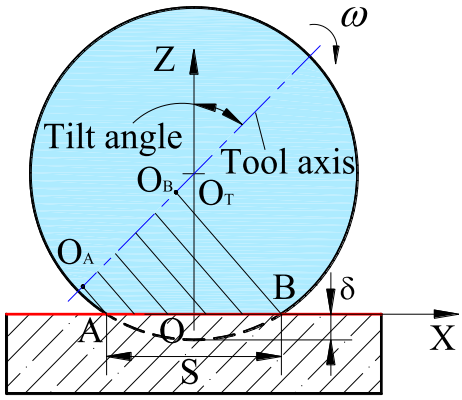

Fig. 2. Schematic diagram of the rotation radius.

Any workpiece surface can be approximated locally by a convex, concave or flat geometry. The material removal models are different for these three shapes, since the contact conditions between the workpiece and the polishing tool are different leading to varying deformations of the polishing tool.

Fig. 3 illustrates the contact state of the polishing tool with a convex surface and a concave surface. The compliant polishing tool is pressed on the rigid part surface. Surface of the tool has a good fit with the part surface shown as the red line. Cartesian coordinates O-XYZ and O'-X'Y'Z' are established, as shown in Fig. 3. Plane XOY is the common tangent plane with the origin at the contact centre on the surface of the part. Plane X'O'Y' is parallel to plane XOY and passes through point (x, y) in the contact area. Distance h', as shown in Fig. 3, can be obtained according to the following geometrical relations:

$$h' = \delta \pm |OO'| \tag{5}$$

where '+' applies to concave surface, and '-' applies to convex surface. h' represents the coordinates of Z axis of point (x, y). $|OO'|$ is the distance between origin point O and O', which can be expressed as Eq. (6) supposing that the curvature centre of the part at the contact point locates on Z axis.

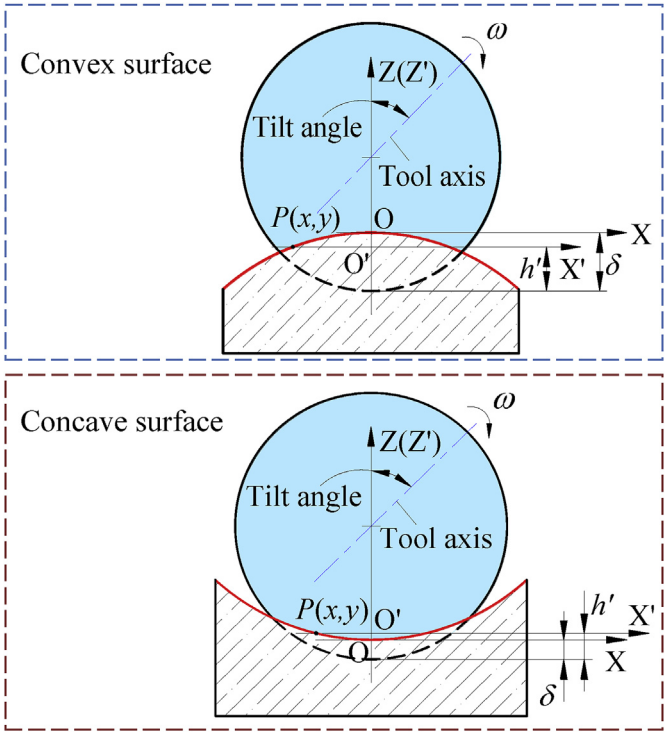

Fig. 3. Contact state of convex/concave surface with polishing tool.

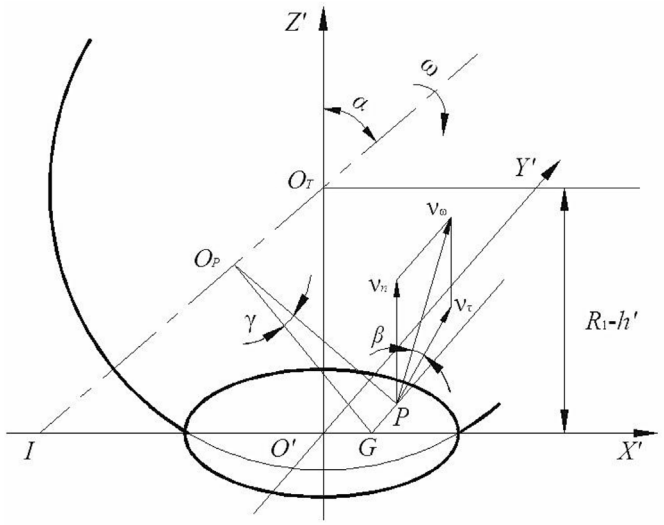

Fig. 4. Illustration for the calculation of the rotation radius and velocity v_ω.

$$|OO'| = R_2 - \sqrt{R_2^2 - x^2 - y^2} \tag{6}$$

where R_2 is the curvature radius of the part at the contact point. In addition, δ expresses the maximum deflections of the polishing tool as they approach each other. The expression of deflection δ is given through the following equation [25]:

$$\delta = \frac{3kFK(k')}{2\pi}\left(\frac{A+B}{b/\Delta}\right) \tag{7}$$

Fig. 4 shows a schematic diagram of the rotation radius of a point P *with a coordinates of* (x, y) with the origin locating at the contact centre. Here, O_T is the geometric centre of the polishing tool, α is the inclination angle of the polishing tool axis, and the tilt direction is towards the X′ axis. The polishing tool rotates at a constant speed ω. In addition, O_P is the rotation centre of point P. Therefor, relative velocity caused by the tool rotation can be given as:

$$v_\omega = \omega \cdot L \tag{8}$$

In right triangle O_PGP, length of the hypotenuse O_PP can be expressed as

$$L = |O_PP| = \sqrt{|O_PG|^2 + y^2} \tag{9}$$

In right triangle O_PGI, length of line O_PG can be given by

$$|O_PG| = \cos\alpha \times (|IO'| + x) \tag{10}$$

In right triangle O_TIO', length of line IO' can be obtained by

$$|IO'| = \tan\alpha \times (R_1 - h') \tag{11}$$

Therefore, the rotation radius of a point (x, y) in the contact area can be expressed as

$$L = |O_PG| = \sqrt{[(R_1 - h')\sin\alpha + x\cos\alpha]^2 + y^2} \tag{12}$$

The rotation of the tool leads to relative motion between the tool head and the part. $\boldsymbol{v_\omega}$ is the velocity vector at point P generated by self-rotating motion of the polishing tool. It can be written as

$$v_\omega = \omega \cdot L = \omega\sqrt{[(R_1 - h')\sin\alpha + x\cos\alpha]^2 + y^2} \tag{13}$$

The direction of the relative velocity $\boldsymbol{v_\omega}$ is perpendicular to the rotation radius O_PP, and $\boldsymbol{v_\omega}$ lies on the plane formed by O_PP and O_PG. In addition, $\boldsymbol{v_\omega}$ can be decomposed along two orthogonal directions as the tangential velocity $\boldsymbol{v_\tau}$ and the normal velocity $\boldsymbol{v_n}$ shown as Fig. 5. Only the tangential component of relative velocity on the polishing area

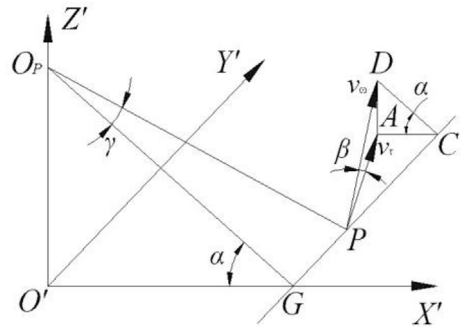

Fig. 5. Illustration for the calculation of tangent velocity v_τ.

affects the local removal rate [13].

Fig. 5 shows an illustration of calculating the tangent component velocity $\boldsymbol{v}_\tau$. Lines O_PG, O_PP, PD, and DC lie in the same plane formed by O_PP and O_PG. Line GC is the intersection of planes O_PGC and $O'X'Y'$. In addition, PD represents the direction of the relative velocity $\boldsymbol{v}_\omega$, and PD is perpendicular to O_PP. Line DC is parallel to line O_PG. The tangent velocity can then be given by

$$v_\tau = v_\omega \cdot \cos\beta \tag{14}$$

where β is the angle between vector $\boldsymbol{v}_\omega$ and $\boldsymbol{v}_\tau$. Owing to the geometrical relationship shown in Fig. 5, this angle can be given by

$$\cos\beta = {PA}/{DP} \tag{15}$$

In right triangle PAC, PA can be expressed as

$$PA = \sqrt{PC^2 + AC^2} \tag{16}$$

In right triangle DPC, PC can be obtained by

$$PC = DP \times \cos\gamma \tag{17}$$

In right triangle DAC, AC can be given as

$$AC = DC \times \cos\alpha = DP \times \sin\gamma \cos\alpha \tag{18}$$

Combining Eqs. (15)–(18), it can be derived that:

$$\cos\beta = \sqrt{1 - \sin^2\gamma \sin^2\alpha} \tag{19}$$

where γ is the angle between line O_PP and O_PG, and can be given as

$$\gamma = \arcsin\left(\frac{|y|}{L}\right) \tag{20}$$

Based on the assumptions mentioned above, combine formula (14), (19) and (20) yields

$$v_\tau = \omega\sqrt{y^2\cos^2\alpha + [(R_1 - h')\sin\alpha + x\cos\alpha]^2} \tag{21}$$

2.3. Material removal modelling

Applying formulas (2) and (21) to formula (1), the mathematical model of the material removal depth of a point in the contact area for spot polishing can be obtained as follows:

$$H(x,y) = \Delta t \cdot K\omega R_e E^* \sqrt{y^2\cos^2\alpha + [(R1 - h')\sin\alpha + x\cos\beta]^2} \sqrt{\left(\frac{3F}{2\pi R_e E^*}\right)^{2/3} - x^2 - y^2} \tag{22}$$

According to formula (22), the depth of the material removed is related to the normal force, spindle speed, tilt angle, and physical and geometric characteristics of the polishing tool and workpiece. Material removal profile can be obtained by taking coordinates lying on the section line of the contact area into formula (22). For example, X-X section profile can be obtained by taking $y = 0$ and $x = -a$: a into formula (22), where a is the radius of the contact area.

3. Experimental verification

3.1. Experimental setup

A series of experiments was carried out to verify the effectiveness of the proposed method of MRP modelling. The experiments were conducted on a five-axis NC machine tool, including three linear movement axes and two rotational axes (B- and C-axes). The setup is as shown in Fig. 6. The B-axis fixed on the X-axis provides rotational movement to ensure the tilt angle of the tool axis. The polishing spindle is mounted on the B-axis with a maximum rotational speed of 30, 000 rpm and maximum power of 4.5 kw. A force sensor is mounted between the specimen and a specially designed fixture fixed on the C axis. The force sensor is a FUTEK TH400 with a resolution of 0.01 N, and is used as a feedback to control the normal polishing force. The force exerted on the part is determined based on the polishing depth, which can be adjusted through the up and down movement of the Z-axis.

The specimens are cylinder with a machined size of Ø 60 × 30 mm. The surfaces were turned using a lathe tool to an average roughness of 475 μm. The polishing tool head is a polyurethane ball with a radius of 15 mm covered with a polishing film. The average grain size of the abrasive used is 35 μm. Each experiment was carried out using a new polishing film. The projection of the tool axis on the plane overlaps with the X-axis shown as the enlarged view.

Experiments were carried out under polishing conditions listed in Table 1. Young's modulus E_1 and Passion's ratio v_1 of the polyurethane

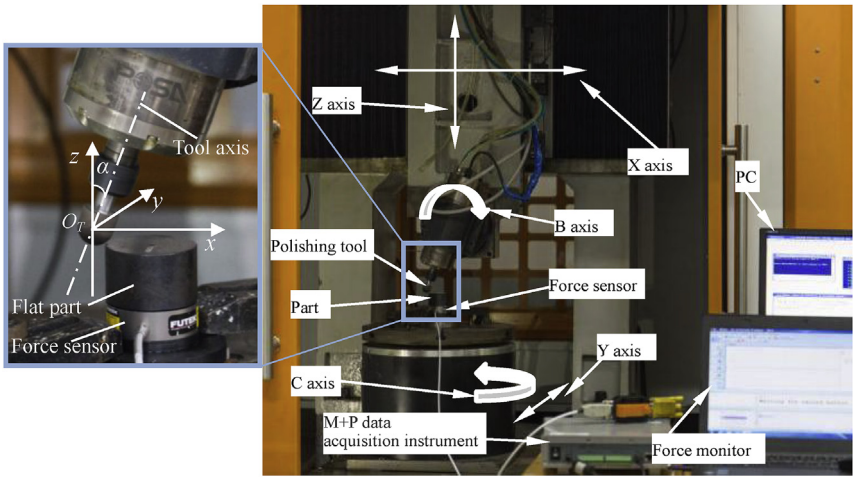

Fig. 6. Experimental set-up.

Table 1
Polishing parameter settings.

Description	Parameters
Polishing tool	E_1 = 5 MPa, υ_1 = 0.3, R_1 = R_1' = 15 mm.
Workpiece	E_2 = 206 GPa, υ_2 = 0.3, R_2 = R_2' = infinite.
Polishing conditions	F = 20N, ω = 2000 rpm, α = 30°, Δt = 5s.

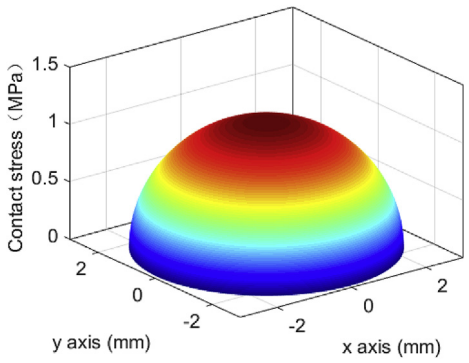

Fig. 7. Distribution of contact stress.

material are 5 MPa and 0.3 with a hardness of Shore A 65 [26]. The material of the workpiece is 40Cr with a hardness of 50 HRC. In addition, E_2 and υ_2 are 206,000 MPa and 0.3 respectively.

3.2. Simulation and experimental results

3.2.1. Contact stress

Formula (2) was simulated with parameters shown in Table 1 to determine the characteristic of the pressure distribution in the contact area. From the result shown in Fig. 7, it can be seen that the pressure mapping is symmetrical about the contact centre. This is consistent with result given in Ref. [17].

3.2.2. Relative velocity

Fig. 8 is the simulation result of the tangent velocity shown as formula (21) with parameters listed in Table 1. Fig. 8 (a) is the top view of the three-dimensional of the velocity distribution. Fig. 8 (b) is the X-X section result and Fig. 8 (c) is the Y-Y section result. In the polishing area, the velocity values are almost the same along Y axis with small level of variation (minimum velocity 2.97 m/s and maximum velocity 3.08 m/s). In the X-X direction, the velocity values in positive X axis are larger than those in negative X axis and the velocity values of points on the X-axis display a linear relationship.

3.2.3. Material removal profile

Formula (22) was simulated using the same polishing parameters shown in Table 1. Fig. 9 (a) shows the experimental data of a polished spot measured by a Keyence 3D Optical Surface Profiler, while Fig. 9 (b) is the material removal distribution predicted by the material removal model of fixed spot polishing. Fig. 9 (c) and (d) are profiles obtained from the predicted and measured 3D data in X-X and Y-Y sectional plane, respectively. The experimental data and simulation results were fitted to determine the Preston coefficient K. Fig. 9 shows that the geometrical profile obtained from material removal model shows a good agreement with the experimental results. This implies that the contact stress and kinematics modelling proposed in this study can provide a reasonable explanation for CCUP with spherical polishing tool.

The profiles both obtained from experiment and simulation show a deviation toward X-axis positive direction which is agreement with the direction of the tool axis inclined. This is because the relative velocity in the contact area is not symmetrical distribution, shown as Fig. 8 (a).

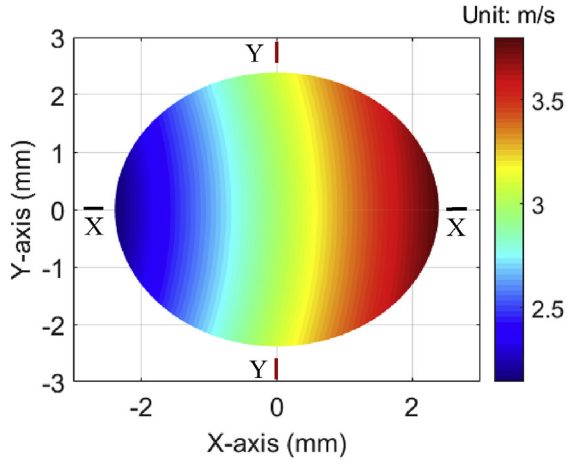

(a) Top view of the simulation result

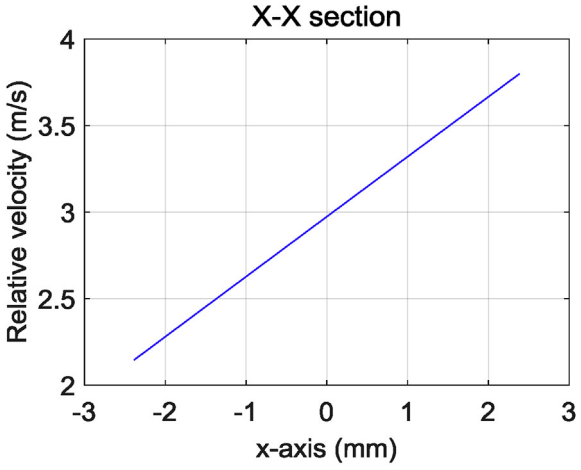

(b) X-X section result

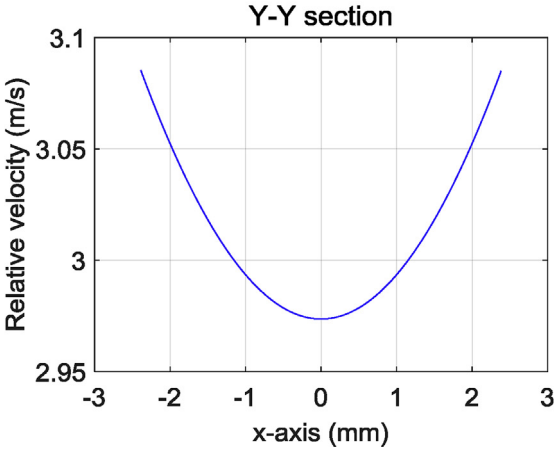

(c) Y-Y section result

Fig. 8. Simulation result of the relative velocity.

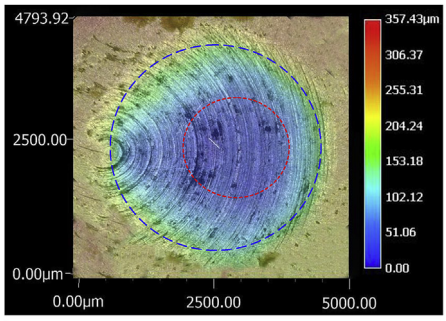

(a) Measured 3D topography data

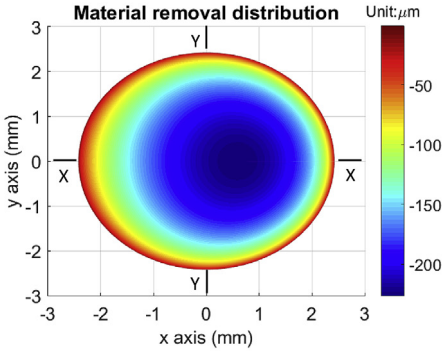

(b) Top view of predicted material removal model

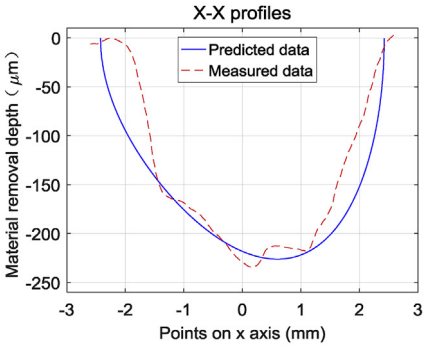

(c) X-X profiles of predicted and measured data

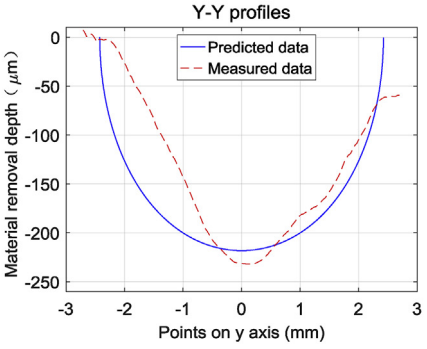

(d) Y-Y profiles of predicted and measured data

Fig. 9. Experimental and predicted results of material removal characteristics.

The material removal depth of a point in the contact area is proportional to the relative velocity and the contact stress which is symmetrical distribution in the contact area illustrated as Fig. 7.

3.3. Evaluation criteria

In this paper, an index is firstly defined to evaluate the deviation degree of the MRP, offering a quantitative description of the deviation characteristics. It is defined as

$$S = \frac{|s_{ld} - s_{rd}|}{s_{ld} + s_{rd}} \times 100\% \tag{23}$$

where S_{ld} is the sum of the material removal depth corresponding with discrete points on the negative X axis, and S_{rd} is the sum of the material removal depth corresponding with discrete points on the positive X axis. The value of S is greater than or equal to 0% and less than hundred-percent. A small value of S represents a probably symmetrical MRP, which is rewarding for uniform material removal in CCUP. The larger the value of S is, the more the inclination of the MRP.

3.4. Results and discussions

3.4.1. Inclination angle

A set of simulations for inclination angles ranging from 10° to 90° are carried out to investigate the effect of the tilt angle on the MRP. The other polishing conditions are $F = 20$ N, $\omega = 2000$ rpm, and $\Delta t = 5$ s. Only points on the X-axis are applied into these simulations. Experiments were conducted with values of inclination angle from 10° to 90°, and other polishing parameters were kept the same. Fig. 10 shows the comparison results of values of S obtained both from simulation and experimental results. The value of S decreases significantly as the inclination angle increases. This means a larger inclination angle leads to a more symmetric material removal profile which is favorable for uniform material removal. However, in real polishing process, a larger inclination angle results in a restricted working space causing interference between the polishing tool and the polished part. The experimental results are consistent with the simulation results calculated through formula (22) with a maximum absolute error of 4.13%. For inclination angle larger than 70°, values of S of the measured profiles show larger than the simulation data. This is because that even if the maximum point of the profile falls in the centre of the contact area, there will be a gap between the two sides due to the waviness of the profiles and the measurement error.

3.4.2. Normal force

The normal force plays a key role in the material removal rate. The simulations were conducted with the normal force varied from 10 to 40 N, based on other parameters including ω = 2000 rmp, $\alpha = 30°$, and $\Delta t = 5$ s. Values of S of profiles obtained from simulations and

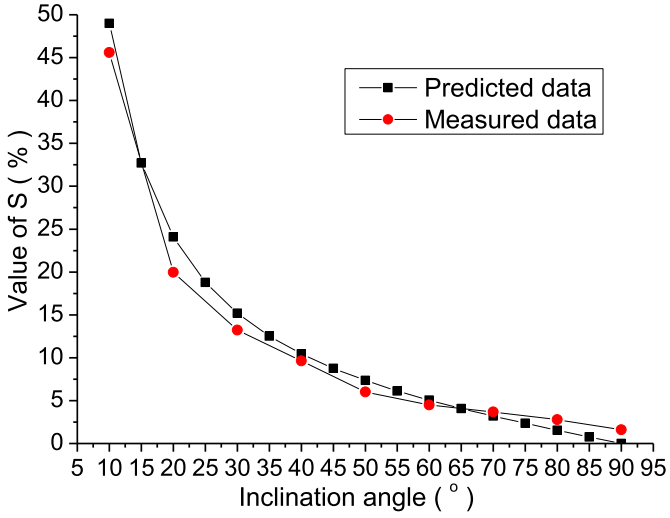

Fig. 10. The effect of inclination angle on the deviation feature of MRP.

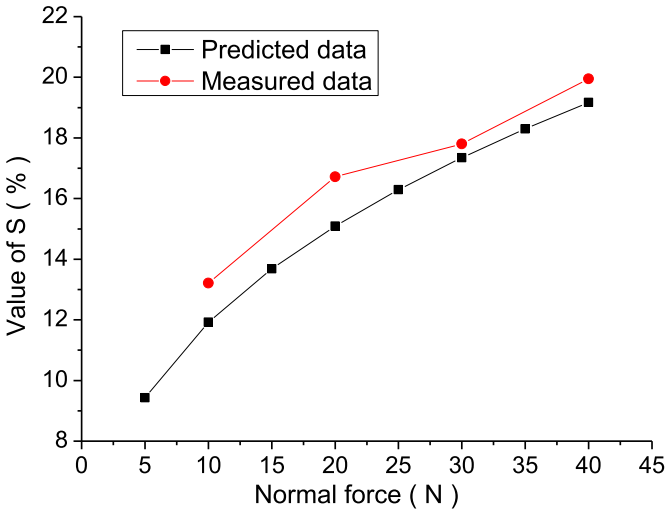

Fig. 11. The effect of normal force on the deviation feature of MRP.

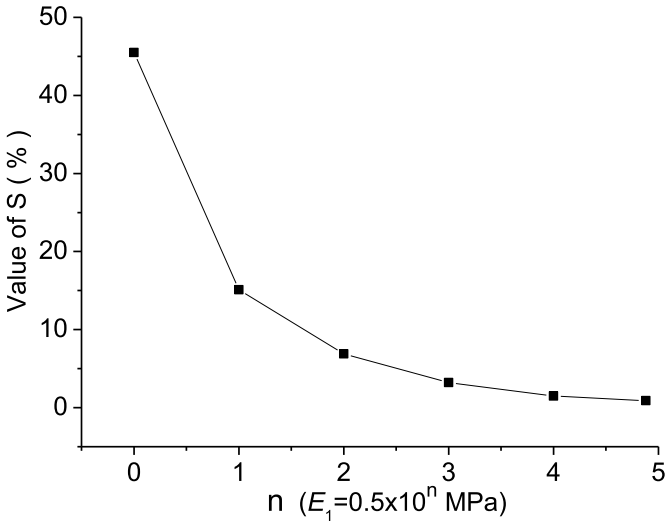

Fig. 12. The effect of modulus of tool on the deviation feature of MRP.

experiments are calculated using formula (23) and are fitted as shown in Fig. 11. There is a big difference between the experimental and simulation results. This may be caused by the vibration and the system error of the machine tool during polishing process. The values of S shows an approximate linear relationship with normal force.

3.4.3. Spindle speed

It is obvious from formula (22) that the material removal depth is proportional to the spindle speed ω. That means spindle speed of the polishing tool significantly affects the relative velocity, but has a little effect on the distribution feature of the MRP in the contact area. The experimental and simulation results indicate that the material removal depth increases as the spindle speed increases, showing a linear relationship between the spindle speed and material removal depth and the value of S has a little change with different values of the spindle speed.

3.4.4. Dwelling time

The material removal mechanism of polishing process is quite different from that of other ultra-precision machining processes such as single point diamond turning and raster milling. With the model of material removal, the polishing tool can be commanded where it should stay longer or shorter for moving more or less materials from the surface, respectively [4]. It is found that the removal volume increases linearly with increasing polishing time for all cases and this infers that the material removal rate is constant when using only polishing time as a variable parameter while keeping other parameters constant [17]. Hence, dwelling time of polishing process has no effect on the deviation feature of the MRP.

3.4.5. Physical feature of the tool material

The shape of the MRP is also determined by the physical properties of the polishing tool material. Simulations were conducted with parameter E_1 as the single variable other parameters kept constant. Value of S of the simulation results are shown in Fig. 12. It shows that the value of S decreases sharply as the modulus increases. It is obvious that a larger modulus leads to a smaller value of S which means a less skewed profile. It can be inferred that a rigid polishing tool generates a parabolic material removal profile. However, in real polishing processes, a compliant polishing tool is much more advantageous because the tool compliance allows for a certain degree of misalignment between the tool and the part [27].

Experiments were carried out using a rigid ball sintered with a CBN abrasive and resin with a radius of 15 mm. The Young's Modulus of the rigid polishing tool was taken as 38000 Mpa [25] in simulation. Fig. 13

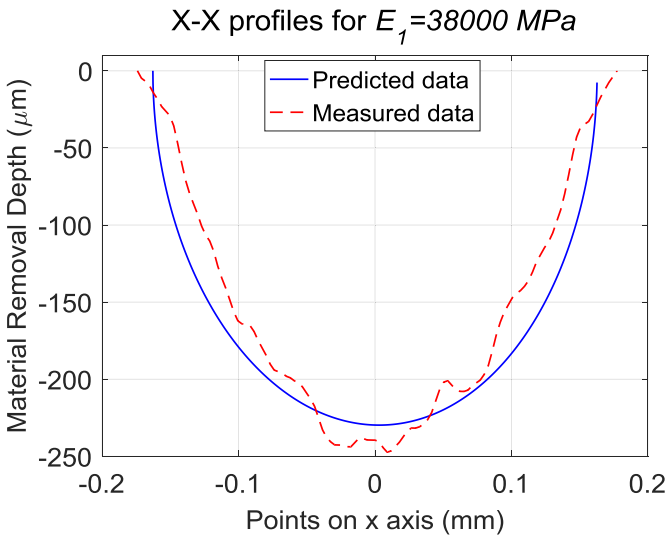

Fig. 13. Measured and predicted data of material removal profile with E_1 = 38000Mpa.

shows material removal profiles obtained from both the simulation and experiment. It can be seen that the material removal profiles are symmetric. This is because there is a much smaller contact area and deformation for contact between a rigid tool head and the polished part.

3.4.6. Inclination direction of the tool axis

Fig. 14 is an illustration of the relationship between the tool posture and the tool path. The projection of the tool axis on plane XOY overlaps with X′ axis which is the tangent line of the tool path I at the contact point at the same time. For tool path II, the projection of the tool axis is perpendicular to the tangent line of the tool path which is overlaps with Y′ axis. Simulation and experiment results indicate that relationship between the inclination direction of the tool axis and the tool path has a coupling effect on the deviation characteristics of material removal profile. A symmetric material removal profile can be obtained with the inclination direction of the tool axis is parallel to the tangent line of the tool path at the point of contact. This can be explained that when polishing along tool path I, the material removal profile orthogonal to the tool path is the Y-Y section profile of fixed spot polishing. It can be inferred that when the projection of the tool axis is perpendicular to the tangent line of the tool path at the contact point shown as tool path II, the material removal profile has the same deviation feature with that of

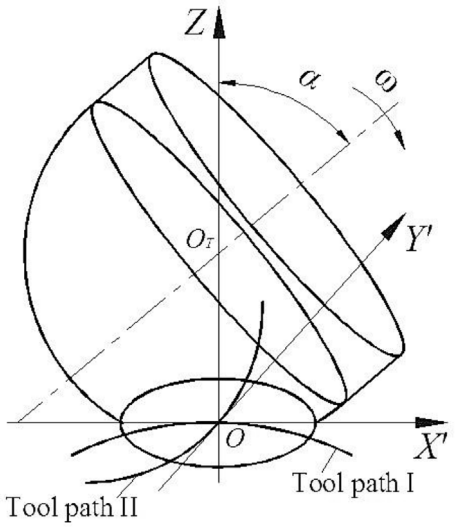

Fig. 14. Illustration of the tool posture. (a) Measured 3D topography data of polishing along a curved tool path. (b) Measured data orthogonal to the tool path.

X-X section profile of spot polishing.

Fig. 15 (a) is a measured 3D data of a segment of material removal along a curved tool path with the projection of the tool axis overlap with the tangent line of the tool path. Fig. 15 (b) is the profile measured along a line orthogonal to the tool path. It can be seen that the MRP is approximate symmetric with the maximum material removal depth locates at the contact centre.

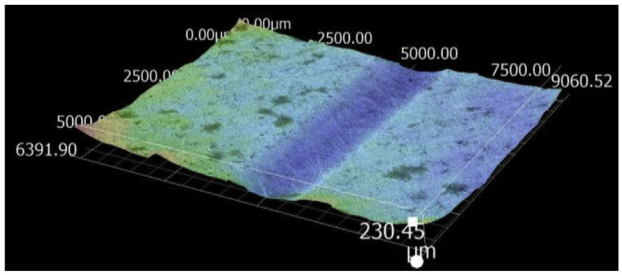

(a) Measured 3D topography data of polishing along a curved tool path

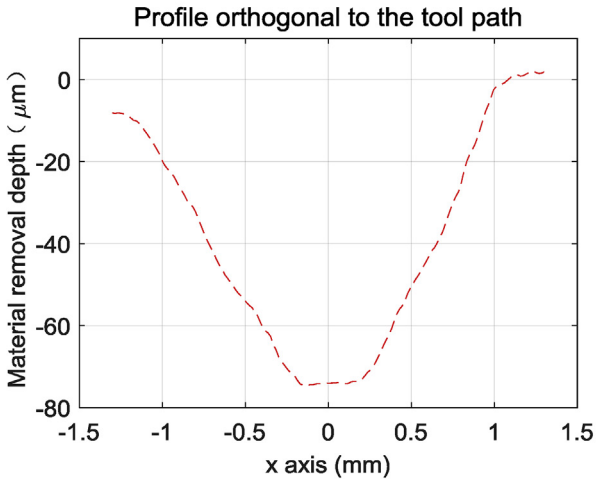

(b) Measured data orthogonal to the tool path

Fig. 15. Experimental results of polishing along a curved tool path.

Table 2
Processing parameters and their levels.

Main effect parameter	Level 1	Level 2	Level 3
A Normal force: F (N)	10	20	30
B Spindle speed: ω (rpm)	1600	2000	2400
C Inclination angle: α (°)	10	20	30
D Tool modulus: E_1 (MPa)	7.8	200	30800

Table 3
L_9 (3^4) orthogonal array used in Taguchi method.

Test	A	B	C	D	Value of S (%)
1	1	1	1	1	33.7
2	1	2	2	2	5.5
3	1	3	3	3	0.7
4	2	1	2	3	1.3
5	2	2	3	1	13.0
6	2	3	1	2	14.3
7	3	1	3	2	5.0
8	3	2	1	3	3.0
9	3	3	2	1	23.7

3.4.7. L_9 orthogonal array

Taguchi method was used to design the simulation experiments in order to estimate the relative significance of each process parameters on the deviation characteristic of the MRP and obtained a parameter optimization strategy for uniform material removal. Table 2 shows the four control factors each with three levels, while the other parameters are kept the same.

Table 3 is the L_9 (3^4) orthogonal array used in Taguchi method. Each group of the parameters were taken into Eq. (22) and S value of X-X profile was taken as the result of the experiments.

The result of the experiments are analyzed using visual method and listed in Table 4. The value of range was calculated using the mean value μ of each level for different parameters and it indicates how the significant factors affect the deviation characteristics of the MRP. It is evident that modulus of the polishing tool is the most significant contributor with a higher modulus resulting in a smaller value of S. Inclination angle is the second major factor that affects the deviation characteristics of the MRP. Normal force and spindle speed have a minimal effect on the deviation characteristics of the MRP that can be neglected compared with that of modulus and inclination angle.

3.4.8. Modulus and inclination angle analysis

Modulus of the polishing tool material and the inclination angle are two significant factors that effect the skewed characteristics of the MRP. A series of simulations was conducted with different value of modulus and inclination angle in order to obtain a more specific and accurate conclusion. The mould of compliant polishing tools always made of polyurethane or rubber. Table 5 presents several kinds of polyurethane with different hardness and modulus and rubber with a modulus of 7.8 MPa. Simulations were carried out for each material with different inclination angles varying from 10º to 90° with a pitch of 5°. The simulation results are shown as Fig. 16 with the y-axis representing the skewed degree of the MRP. The result shows an obvious trend that a larger inclination angle and modulus result in a smaller value of *S*.

Table 4
Result of visual analysis method.

Parameters	Level 1 μ (%)	Level 2 μ (%)	Level 3 μ (%)	Range R (%)
A	13.3	9.5	10.6	3.8
B	13.3	7.2	12.9	6.1
C	17.0	10.2	6.2	10.8
D	23.5	8.3	1.7	21.8

Table 5
Modulus and the corresponding hardness of the polishing tool material.

	Polyurethane					Rubber
					Shore D hardness	
Shore A hardness	65	80	90	93	70	
Modulus (MPa)	5	20	60	200	600	7.8

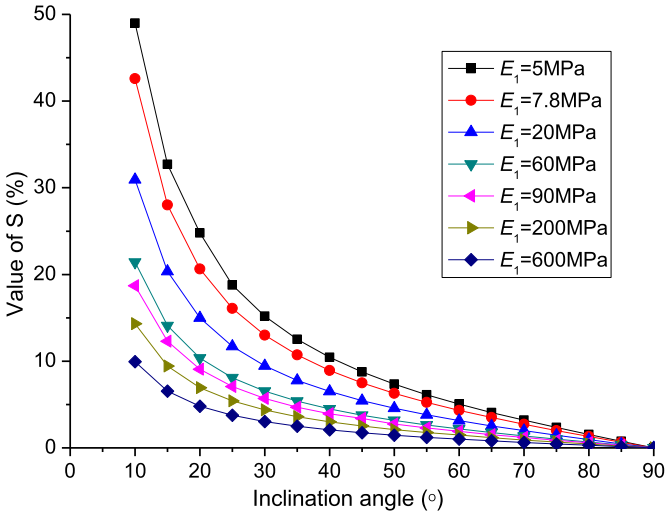

Fig. 16. Simulation result for inclination angles with different value of E_1.

4. Conclusions

In this paper, a material removal model of surface polishing was established to investigate the effects of the polishing parameters on the deviation characteristics of the MRP. Simulations and experiments were carried out to analyze the characteristics of the material removal through surface polishing. The following conclusions can be drawn for obtaining a symmetrical MRP.

(1) If it is possible to ensure the projection of the tool axis parallel to the tangent line of the tool path at the contact point, a symmetric material removal profile can be obtained. For a curved tool path with variable curvature, this polishing condition is difficult to realize limited by the acceleration of the polishing machine tool or robotic. Then following conclusion must be helpful.
(2) The result of the Taguchi method indicates that the modulus and the inclination angle of the tool axis are the two major factors that determine the shape of the MRP. Normal force and spindle speed have little effect on the deviation feature of the MRP.
(3) Simulation and experimental results indicates that the deviation degree of MRP decreases with the increasing of the inclination angle. That means a larger inclination angle is more favorable for a symmetrical material removal profile. However, in real polishing processes, the tilt angle should be chosen considering the working space of CCUP.
(4) Simulation result shows that the deviation feature of the MRP is significantly affected by the modulus of the polishing tool. A softer tool head leads to a more skewed material removal profile. A rigid polishing tool brings in a parabolic profile in any section which is favorable for path planning and ensuring uniform material removal, and at the same time, results in a larger material removal depth and a smaller contact area. For example, a polishing tool with a modulus of 60 MPa can obtain a MRP with the S value of 5% theoretically using an inclination angle of 60°

The work is potentially useful for the planning of the tool path and the tool posture of CCUP.

Acknowledgement

This work was supported by the National Natural Science Foundation of China (grant number 51375379) and Shaanxi Province key projects (grant number 2017ZDXM-GY-133).

Appendix A. Hertz contact theory

$$P(x,y) = P_0\sqrt{1-(\frac{x}{a})^2-(\frac{y}{b})^2} \tag{24}$$

where P_0 is the maximum contact pressure located at the centre of the contact ellipse. It is given by

$$P_0 = \frac{b}{E(k')\Delta} \tag{25}$$

$$b = \sqrt[3]{\frac{3kE(k')}{2\pi}(F\Delta)} \tag{26}$$

$$\Delta = \frac{1}{A+B}(\frac{1-\upsilon_1^2}{E_1}+\frac{1-\upsilon_2^2}{E_2}) \tag{27}$$

$$A = \frac{1}{4}(\frac{1}{R_1}+\frac{1}{R'_1}+\frac{1}{R_2}+\frac{1}{R'_2}) - \frac{1}{4}\sqrt{[(\frac{1}{R_1}-\frac{1}{R'_1})+(\frac{1}{R_2}-\frac{1}{R'_2})]^2-4(\frac{1}{R_1}-\frac{1}{R'_1})(\frac{1}{R_2}-\frac{1}{R'_2})\sin^2\phi} \tag{28}$$

$$B = \frac{1}{4}(\frac{1}{R_1}+\frac{1}{R'_1}+\frac{1}{R_2}+\frac{1}{R'_2}) + \frac{1}{4}\sqrt{[(\frac{1}{R_1}-\frac{1}{R'_1})+(\frac{1}{R_2}-\frac{1}{R'_2})]^2-4(\frac{1}{R_1}-\frac{1}{R'_1})(\frac{1}{R_2}-\frac{1}{R'_2})\sin^2\phi} \tag{29}$$

One additional equation is needed to determine the value of $k = b/c$, namely,

$$\frac{B}{A} = \frac{\frac{1}{k^2}E(k')-K(k')}{K(k')-E(k')} \tag{30}$$

$$k' = \sqrt{1-k^2} \tag{31}$$

$E(k')$ and $K(k')$ are complete elliptic integral of the first and second kind, respectively.

Appendix B. Supplementary data

Supplementary data related to this article can be found at https://doi.org/10.1016/j.precisioneng.2018.08.020.

References

[1] Márquez JJ, Pérez JM, Rıos J, et al. Process modeling for robotic polishing. J Mater Process Technol 2005;159(1):69–82.
[2] Rolland JP, Thompson KP. Freeform optical surfaces: a revolution in imaging optical design. Opt Photon News 2012;23(6):30–5.
[3] Xu P, Cheung CF, Li B, et al. Kinematics analysis of a hybrid manipulator for computer controlled ultra-precision freeform polishing. Robot Comput Integrated Manuf 2017;44:44–56.
[4] Cheung CF, Kong LB, Ho LT, To S. Modeling and simulation of structure surface generation using computer controlled ultra-precision polishing. Precis Eng 2011;35:574–90.
[5] Xi F, Zhou D. Modeling surface roughness in the stone polishing process. Int J Mach Tools Manuf 2005;45:365–72.
[6] Lee HS, Jeong HD, Dornfeld DA. Semi-empirical material removal rate distribution model for SiO_2 chemical mechanical polishing(CMP) processes. Precis Eng 2013;37:483–90.
[7] Kim DW, Kim SW. Static tool influence function for fabrication simulation of hexagonal mirror segments for extremely large telescope. Optic Express 2005;13:910–7.
[8] Jin M, Ji S, Pan Y, Ao HP, Han SF. Effect of downward depth and inflation pressure on contact force of gasbag polishing. Precis Eng 2016;47:81–9.
[9] Oba Y, Kakinuma Y. Simultaneous tool posture and polishing force control of unknown curved surface using serial-parallel mechanism polishing machine. Precis Eng 2017;49:24–32.
[10] Moumen M, Chaves-Jacob J, Bouaziz M, et al. Optimization of pre-polishing parameters on a 5-axis milling machine. Int J Adv Manuf Technol 2016;85(1):1–12.
[11] Feng D, Sun Y, Du H. Investigations on the automatic precision polishing of curved surfaces using a five-axis machining centre. Int J Adv Manuf Technol 2014;72(9):1625–37.
[12] Wang G, Zhou X, Meng G, et al. Modeling surface roughness for polishing process based on abrasive cutting and probability theory. Mach Sci Technol 2017:1–13.
[13] Yang MY, Lee HC. Local material removal mechanism considering curvature effect in the polishing process of the small aspherical lens die. J Mater Process Technol 2001;116:298–304.
[14] Zhang L, Tam HY, Yuan CM, Chen YP, Zhou ZD. An investigation of material removal in polishing with fixed abrasive. Proc Inst Mech Eng 2002;216(1):103–12.
[15] Tam HY, Cheng HB. An investigation of the effects of the tool path on the removal of material in polishing. J Mater Process Technol 2010;210(5):807–18.
[16] Fan C, Zhao J, Zhang L, Wong YS, Hong GS, Zhou WS. Modeling and analysis of the MRP for free abrasive polishing with sub-aperture pad. J Mater Process Technol 2014;214:285–94.
[17] Cao ZC, Cheung CF, Zhao X. A theoretical and experimental investigation of material removal characteristics and surface generation in bonnet polishing. Wear 2016;360–361:137–46.
[18] Schinhaerl M, Rascher R, Stamp R, et al. Utilisation of time-variant influence functions in the computer controlled polishing. Precis Eng 2008;32(1):47–54.
[19] Tsai MJ, Huang JF, Kao WL. Robotic polishing of precision molds with uniform material removal control. Int J Mach Tools Manuf 2009;49(11):885–95.
[20] Kim DW, Kim SW. Static tool influence function for fabrication simulation of hexagonal mirror segments for extremely large telescopes. Opt Express 2005;13(3):910–7.
[21] Preston FW. The theory and design of plate glass polishing machines. Soc Glass Technol 1927;11:214–56.
[22] Roswell A, Xi F, Liu G. Modelling and analysis of contact stress for automated polishing. Int J Mach Tools Manuf 2006;46(3–4):424–35.
[23] Bhushan B. Contact mechanics of rough surfaces in tribology: multiple asperity contact. Tribol Lett 1998;4(1):1–35.
[24] Wang G, Wang Y, Xu Z. Modeling and analysis of the material removal depth for stone polishing. J Mater Process Technol 2009;209(5):2453–63.
[25] Schmidt Richard J. Advanced mechanics of materials. Prentice Hall; 1998.
[26] Liu HJ. Handbook of polyurethane elastomer. M. Chemical Industry Press; 2012. p. 196–7.
[27] Liao L, Xi F, Liu K. Modeling and control of automated polishing/deburring process using a dual-purpose compliant toolhead. Int J Mach Tools Manuf 2008;48(12–13):1454–63.